

On the crystallization onset in white dwarfs

D. A. Baiko*

Ioffe Institute, Politekhnicheskaya 26, 194021 Saint Petersburg, Russia

Received/accepted

ABSTRACT

Thermal evolution of the central region of a $0.9 M_{\odot}$ C/O white dwarf at the initial stage of the ion mixture crystallization is studied by numerically solving the heat equation on a fine spatial and temporal grid and by including a detailed treatment of the latent heat release. Formation of two spherical shells is observed. The outer one surrounds a region where crystallization has begun. The inner one bounds a fully solidified core which has exhausted its latent heat. The region between the shells is partially liquid and partially solid. It gradually emits the latent heat of crystallization and also it releases light elements (carbon) in the process of element redistribution, accompanying the mixture solidification. Assuming that all released light elements cross the outer shell, we have estimated their flux induced by the mixture crystallization. The resulting flux is not divergent and is much smaller than an estimate derived from the growth rate of the fully crystallized core.

Key words. stars: evolution – stars: white dwarfs – stars: interiors – dense matter – plasmas – convection

1. Introduction

The origin of strong magnetic fields in white dwarf stars (WD) is a hot topic of modern astrophysics (e.g. Bagnulo & Landstreet 2022). In particular, a debate is ongoing on whether the magnetic field can be generated in a WD core via crystallization driven convection and dynamo and whether it can subsequently emerge and be observed at the stellar surface (e.g. Isern et al. 2017; Ginzburg et al. 2022; Fuentes et al. 2023; Montgomery & Dunlap 2024; Blatman & Ginzburg 2024, and references therein). Most recently, Fuentes, Castro-Tapia & Cumming (2024) have proposed a short-lived ($\lesssim 10$ Myr) phase of compositionally driven convection characterized by a large upward light element flux and rapid fluid motions, operating at the initial stage of C/O WD crystallization. Lanza et al. (2024) discussed a powerful dynamo driven by rapid upward flow of ^{22}Ne -depleted solid flakes in the process of ^{22}Ne distillation prior to core crystallization in C/O/ ^{22}Ne WD.

The present paper focuses on crystallizing C/O WD. We study the thermal evolution of matter in the inner core region at the freezing onset by numerically solving the heat equation on a fine spatial and temporal grid and by including a detailed treatment of the latent heat release. As a by-product, we obtain an alternative estimate of the light element flux induced by the C/O mixture crystallization.

2. Model

When freezing of a WD core begins, the very central region reaches its crystallization temperature and then it cannot cool further¹ unless all of its latent heat has been released and re-

moved. The release of the latent heat is controlled by the ability of the system to carry it away, that is by available thermal gradients and heat fluxes. As the time goes on, more outward layers also reach their crystallization temperature and start releasing latent heat i.e. the region that has begun crystallization gradually expands. At some point, the central part completely exhausts its latent heat and resumes cooling according to the standard heat equation. Thus, in general, once crystallization in a WD begins, there are three regions. In the inner and outer regions, matter cools according to the standard heat equation being, respectively, in a crystal or liquid state. The intermediate region represents a reservoir of heat, where matter is partially solid and partially liquid, its temperature being equal to the local crystallization temperature². To model the intermediate region, one simply has to keep track of the balance between the total amount of available heat and incoming and outgoing heat fluxes.

Since we are mostly interested in a qualitative picture of the freezing onset, our model is significantly simplified. Following Fuentes et al. (2024), we assume a specific form of the mass density ρ dependence on the radial coordinate r :

$$\rho = \rho_c \left(1 - \frac{r^2}{R_{\text{WD}}^2} \right)^{3/2}, \quad (1)$$

where $\rho_c = 1.86 \times 10^7$ g/cc is the central density and $R_{\text{WD}} = 6371$ km is the WD radius. The specific values are taken from the evolutionary model³ of a WD with a thick hydrogen envelope and a mass of $M_{\text{WD}} = 0.9 M_{\odot}$ near the crystallization onset (Bédard et al. 2020, the reference model).

We further assume equal proportions by mass of C and O but neglect any effects of phase separation and element redistribution, including the gravitational energy release, on thermal evolution. In reality, the liquid around newly forming crystals gets depleted of the heavier element (oxygen) and enriched

² This is similar to a water-ice mixture at 0°C .

³ <https://www.astro.umontreal.ca/~bergeron/CoolingModels>

* E-mail: baiko.astro@mail.ioffe.ru

¹ This statement is obvious for dense matter composed of a single ion sort. For an ionic mixture, it is true, if the ion composition of the freezing liquid remains fixed. In what follows, we shall make this assumption as it is inherent in the effect to be considered (see below).

with the lighter element (carbon). This creates compositionally driven instability conditions discussed e.g. by Fuentes et al. (2023); Montgomery & Dunlap (2024), resulting in the light element flux F_X directed upward and an opposite heavy element flux, which replenishes the oxygen content of the liquid. Since we limit our consideration to the inner core region and to initial stages of crystallization, we do not describe these effects in detail except for estimating the flux F_X and adopting the fixed liquid composition assumption. We expect that these effects, particularly the extra heat, produced by mixing, which also has to be removed, could only strengthen our conclusions. Furthermore, we neglect any effects associated with distillation of ^{22}Ne (Isern et al. 1991; Blouin, Daligault & Saumon 2021) or any other heavier species.

The crystallization (melting) temperature T_m is calculated as

$$T_m = \frac{Z_1^{5/3} e^2}{a_e k_B \Gamma_{1m}} \xi_{\text{CO}}(3/7), \quad (2)$$

where $Z_1 = 6$ is the carbon charge number, $a_e = (4\pi n_e/3)^{-1/3}$, n_e is the electron density, $\Gamma_{1m} = 175.6$ is the Coulomb coupling parameter of a classic one-component plasma at melting (Baiko & Chugunov 2022), and $\xi_{\text{CO}}(3/7) = 1.05$ is a correction at the oxygen number fraction $x_O = 3/7$ based on the phase diagram of the C/O mixture (Blouin & Daligault 2021).

Furthermore, we assume a constant heat capacity $C = 2.7k_B$ per ion, which is a reasonable approximation for mildly quantum liquids and solids (in our system, ion plasma temperature is ~ 3 times greater⁴ than the actual temperature) in the vicinity of the phase transition (cf. Baiko & Chugunov 2022); constant thermal conductivity $\kappa = 1.2 \times 10^{16} \text{ erg cm}^{-1} \text{ s}^{-1} \text{ K}^{-1}$ based on the electron-ion collision frequency calculation, fit, and extrapolation to mixtures (Potekhin et al. 1999); and the latent heat of crystallization for the classic equimass C/O mixture, $\lambda = 0.67 k_B T_m$ per ion (Baiko 2023).

Realistic study of the crystallization onset implies a description of the local latent heat release and removal which requires a non-isothermal approach. In our model, the initial temperature at the stellar center is taken to be 0.03% greater than the melting temperature $T_m(0)$. The initial temperature profile, $T_{\text{ini}}(r)$, is based on the following scaling:

$$T_{\text{ini}}(r) = 1.0003 T_m(0) - 0.5K r^2, \quad (3)$$

$$K = \frac{\rho C}{3\kappa \langle A \rangle m_u} \left| \frac{dT}{dt} \right|,$$

where $\langle A \rangle$ is the average mass number of the mixture, m_u is the atomic mass unit, and dT/dt is a time derivative of temperature.

We analyze thermal evolution of matter only out to $r = r_0$ with $r_0 = 3000 \text{ km}$ to avoid the need to describe complicated physics of the outer, partially ionized and partially degenerate layers. Consequently, a boundary condition at r_0 is required and for that we specify the time derivative of temperature, $dT(r_0)/dt = \alpha_0(t)$. In principle, the true form of $\alpha_0(t)$ can be obtained only from a full-star evolutionary modeling with a high-level code and with account of the effects investigated in the present paper. In the absence of that, we can, first, assert that $T(r_0)$ monotonously decreases with t and, second, take advantage of the fact that we are actually interested in a relatively brief time interval $\Delta t < 100 \text{ Myr}$ since the crystallization onset, which

⁴ The ion plasma temperature $T_p \equiv \hbar \omega_p / k_B \approx 2.2\theta_D$, where ω_p is the ion plasma frequency and θ_D is the Debye temperature. At $T_p/T \gg 1$, one-component ion plasma is known to be in the regime of strong ion quantum effects.

covers the purported efficient convection stage. For this reason, the time derivative is assumed to be constant $\alpha_0 = -1.5 \times 10^{-10} \text{ K/s}$. This value of α_0 is close to the average time derivative of the central temperature in the reference model shortly *before* the crystallization onset. On the other hand, in our model, such a value of α_0 results in the average time derivative of the central temperature *after* the crystallization onset equal to $-0.83 \times 10^{-10} \text{ K/s}$, which is practically the same as the one in the reference model. Besides that, we have tried several other values of α_0 , bracketing the fiducial value above within a factor of ~ 2 , which, naturally, yielded qualitatively similar picture of the temperature variation. We therefore do not expect that implementing a weak decrease of $|\alpha_0(t)|$ over considered Δt could affect our main conclusions. We have also set dT/dt to α_0 in equation (3).

3. Results

The result of modeling is shown in Fig. 1. Displayed is the temperature profile as a function of r with different curves corresponding to different time stamps. The dotted (red) curve demonstrates the initial profile. Four solid (green) curves between it and the long dashed (blue) profile show the evolution before the latent heat in the center is exhausted: the upper solid curve is separated by 2 Myr from the initial one, the other three curves add 8 Myr of evolution each. On the left-hand side, these solid curves approach and then smoothly merge onto the thick short dashed (orange) line, which is the profile of the crystallization temperature. At $r = 0$, they take the value $T_m(0)$. Hence, in this case, there are only two regions: the inner one is at the local crystallization temperature and the outer one represents the cooling liquid. In the inset, the top-left corner of the graph is shown in more detail. Five (green) solid profiles to the right of the crystallization temperature are separated from each other and from the initial (dotted red) one by 400 kyr.

The long dashed (blue) curve corresponds to 27.6 Myr since the beginning of the simulation, slightly later than the moment at which the crystallization of the innermost core region is complete i.e. all its latent heat is removed. Consequently, the solid (green) curves below it contain three segments, corresponding to the three regions described in the first paragraph of section 2. The segments, describing the cooling crystal with progressively lower central temperatures, can be seen to the left of the crystallization profile. The mutual time separation between these curves is 8 Myr (the dot-dashed green curve is also part of this family, see below) and the upper one of them is at 2 Myr after the long dashed profile. This regime is characterized by an expansion of the region which has reached $T_m(r)$ and of the region which has exhausted its latent heat and cooled below $T_m(r)$. The radial extent of the intermediate region shrinks and by the last curve, which displays the temperature profile at 69.6 Myr, its size becomes smaller than the spatial grid. Five solid (green) curves to the left of the crystallization temperature profile in the inset are separated from each other and from the long dashed (blue) curve by 400 kyr.

For illustration, by dot-dashed curves we show the temperature profile at 45.6 Myr for three sequences with different latent heat values (assuming the same initial profile and boundary condition): the upper one (green) corresponds to the standard λ value, the one in the middle and the lower one (both brown) demonstrate the cases with $\lambda = 0.33 k_B T_m$ and zero latent heat, respectively. For the latter, there should be no difference between the liquid and solid phases in our code, and a smooth curve, cooling rapidly in the center, is in fact obtained.

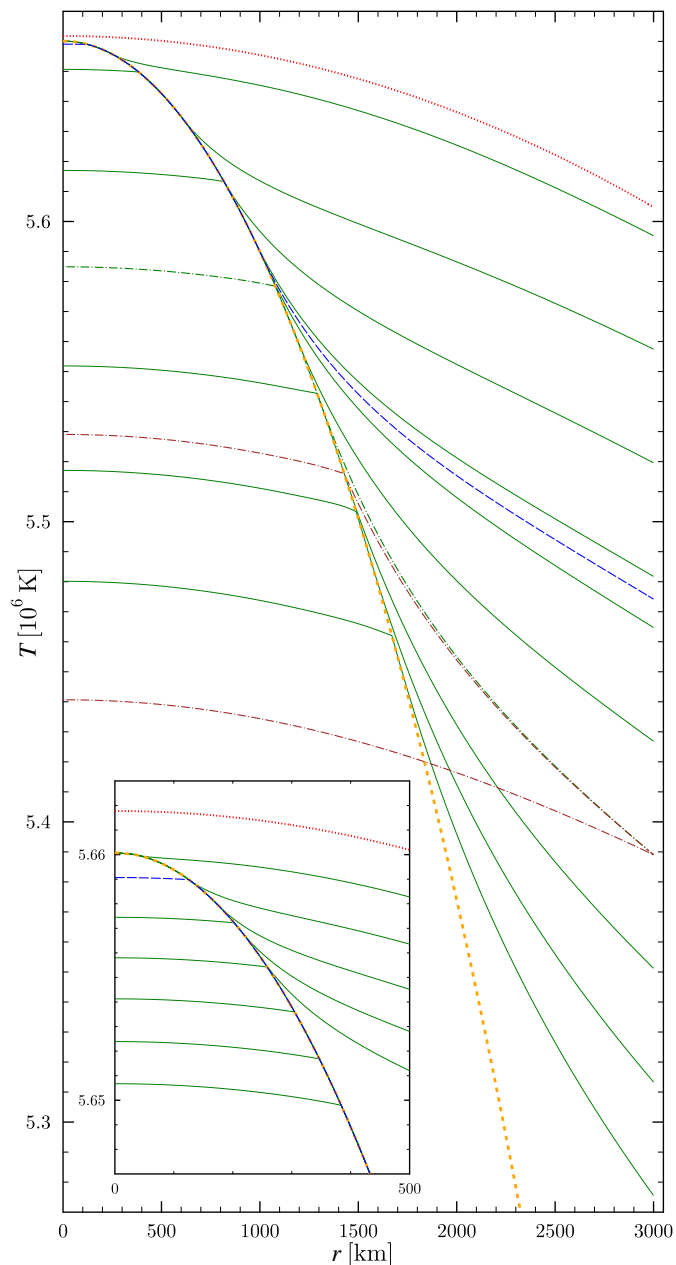


Fig. 1. Internal temperature profile of cooling WD model at various times. Initial profile (dotted red), profile shortly after formation of the fully crystallized core (long dashed blue), three profiles at 45.6 Myr since the beginning of modeling (dot-dashed green for the default latent heat value, dot-dashed brown for two times smaller and zero latent heat values), profiles at other times (solid green, see text for details). Crystallization temperature is shown by thick short (orange) dashes.

In Fig. 2, we show radii of the regions that have started and completed crystallization denoted as r_m and r_c , respectively, by dot-dashed (red) and solid (blue) curves as functions of time. As we observed in Fig. 1, the difference between the initial time stamps for the two processes is ~ 27 Myr. At the beginning, both dependences have infinite time derivative in a qualitative agreement with the analytic model of Fuentes et al. (2024). Eventually, the two curves merge (to within the spatial grid size).

Let us now estimate the flux of light elements, F_X , resulting from phase separation accompanying crystallization (in our case, this is the flux of carbon ions). Fuentes et al. (2024) linked the flux with the velocity of the crystallization front. Specifically, if

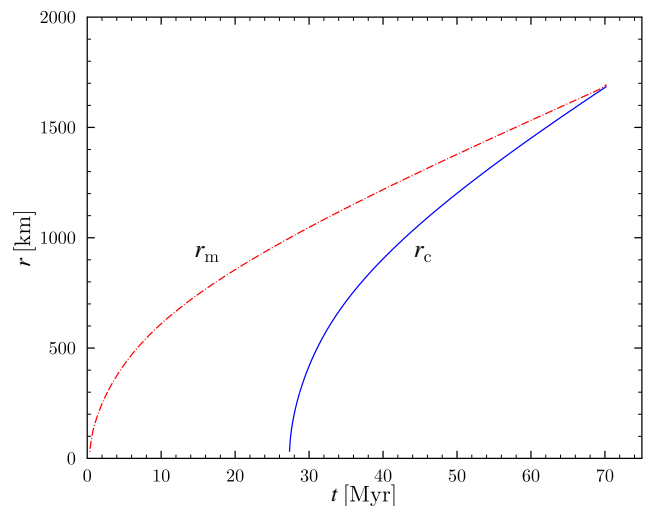


Fig. 2. Radius of the region, which has started crystallization (dot-dashed red), and of the fully crystallized core (solid blue) vs. time since the beginning of modeling.

the front moves from $r - dr$ to r over a time interval dt , then, in their model, the entire spherical shell of thickness dr turns from the liquid to the solid phase. This allows one to calculate the mass of released light elements, which then cross the sphere of the radius r during dt (by convective motions). This quantity was found to be divergent at the initial stages of crystallization.

However, as our solution shows, such a picture does not apply at the crystallization onset. Actually, light elements are released rather slowly within the spherical shell of the outer radius r_m and inner radius r_c ($r_c = 0$ for the first ~ 27 Myr). The mass of released light elements over an interval dt is proportional to the total mass which has solidified. This, in turn, is proportional to the amount of latent heat carried away from this region. If convection is sufficiently rapid, then the light elements can cross the sphere at r_m during dt . This provides an upper estimate of the convective flux.

We have calculated the flux of light elements using both prescriptions and show the results in Fig. 3. Based on the phase diagram of Blouin & Daligault (2021), we have set the difference in the carbon mass fraction between the liquid and the solid to $\Delta X = 0.11$. Dot-dashed (blue) curve assumes that the flux is determined by the fully crystallized core growth rate. In agreement with the analysis of Fuentes et al. (2024), this curve is divergent. Solid (green) curve⁵ takes into account gradual release of light elements controlled by the latent heat removal which has been taking place over ~ 27 Myr before the start of the fully crystallized core formation. In this case, as soon as the central region reaches the crystallization temperature, the flux rapidly grows starting from zero. Then it is everywhere finite, slowly growing, and, even at 10 Myr since the appearance of the fully solidified core, it is more than two times smaller than the previous estimate. At the end of our modeling, r_c catches up with r_m , and both calculations of the light element flux coincide as they should.

4. Conclusion

We have considered thermal evolution of the internal region of a $0.9 M_\odot$ C/O WD over ~ 70 Myr since the beginning of ion

⁵ To reduce discretization artefacts, we applied moving average over $\pm 1\%$ of the current time t .

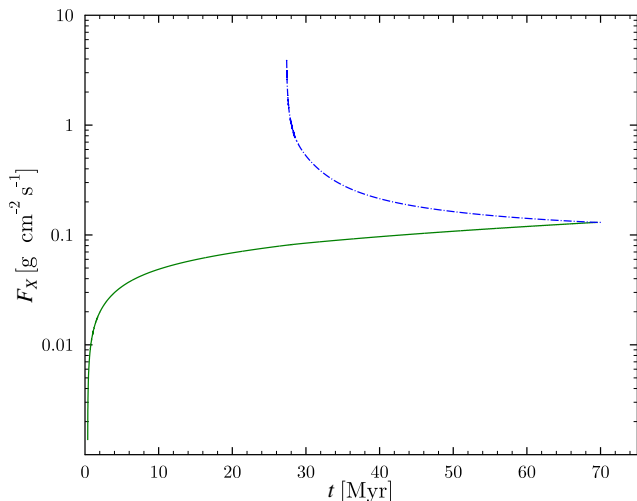


Fig. 3. Light element flux vs. time. Dot-dashed (blue) and solid (green) curves show fluxes based on the fully crystallized core growth rate and on the gradual release of light elements controlled by the latent heat removal, respectively.

plasma crystallization in its center. We have observed formation of two spherical shells. The outer one surrounds the region, where crystallization has begun, whereas the inner one bounds the fully solidified core, which has exhausted its latent heat. The region between the shells is partially liquid and partially solid. It gradually emits the latent heat of crystallization, which is carried away along the existing thermal gradients, and also it releases light elements in the process of element redistribution, accompanying the mixture solidification. The inner shell first appears ~ 27 Myr after the appearance of the outer shell, whose radius reaches ~ 1000 km at this moment. At ~ 70 Myr, the inner shell catches up with the outer one, and the crystallization process adopts the familiar form of a motion of a 2D front.

Assuming that all released light elements cross the outer shell, we have estimated their flux induced by the mixture crystallization. Up until the time when both shells merge, the result obtained is significantly smaller than the estimate based on the model of Fuentes et al. (2024). In particular, according to Fig. 2 of that work, the efficient convection driven by the light element flux is expected to cease after ~ 3 Myr since the formation of the fully solidified core. However, at this moment, the actual flux of light elements is ~ 5 times lower than the Fuentes et al. (2024) prediction and is even lower at earlier times (cf. Fig. 3). This means that the criterion for the efficient convection is not fulfilled at the early stages of WD crystallization and, consequently, such a phenomenon likely does not occur.

Acknowledgements. The author is deeply grateful to D. G. Yakovlev for discussions and to expert referee, Mike Montgomery, for valuable comments. This work has been supported by the Russian Science Foundation grant 24-12-00320.

References

- Bagnulo, S., & Landstreet, J. D. 2022, *ApJL*, 935, L12
 Baiko, D. A., & Chugunov, A. I. 2022, *MNRAS*, 510, 2628
 Baiko, D. A. 2023, *MNRAS*, 522, L26
 Bédard, A., Bergeron, P., Brassard, P., & Fontaine, G. 2020, *ApJ*, 901, 93
 Blatman, D., & Ginzburg, S. 2024, *MNRAS*, 528, 3153
 Blouin, S., Daligault, J., & Saumon, D. 2021, *ApJL*, 911, L5
 Blouin, S., & Daligault, J. 2021, *Phys. Rev. E*, 103, 043204
 Fuentes, J. R., Cumming, A., Castro-Tapia, M., & Anders, E. H. 2023, *ApJ*, 950,

- Fuentes, J. R., Castro-Tapia, M., & Cumming, A. 2024, *ApJL*, 964, L15
 Ginzburg, S., Fuller, J., Kawka, A., & Caiazzo, I. 2022, *MNRAS*, 514, 4111
 Isern, J., Mochkovitch, R., García-Berro, E., & Hernanz, M. 1991, *A&A*, 241, L29
 Isern, J., García-Berro, E., Külebi, B., & Lorén-Aguilar, P. 2017, *ApJL*, 836, L28
 Lanza, A. F., Rui, N. Z., Farihi, J., Landstreet, J. D., & Bagnulo, S. 2024, *A&A*, 689, A233
 Montgomery, M. H., & Dunlap, B. H. 2024, *ApJ*, 961, 197
 Potekhin, A. Y., Baiko, D. A., Haensel, P., & Yakovlev, D. G. 1999, *A&A*, 346, 345